

## Supporting Information

### **Ce-doped Bi based catalysts for highly efficient electroreduction of CO<sub>2</sub> to formate**

De-Huang Zhuo,<sup>a,b</sup> Qing-Song Chen,<sup>\*a</sup> Xiu-Hui Zhao,<sup>a</sup> Yin-Long Jiang,<sup>a</sup> Jian Lu,<sup>a</sup> Zhong-Ning Xu<sup>a</sup> and Guo-Cong Guo<sup>\*a</sup>

<sup>a</sup> State Key Laboratory of Structural Chemistry, Fujian Institute of Research on the Structure of Matter, Chinese Academy of Sciences, Fuzhou, Fujian 350002, P. R. China Email: chenqs@fjirsm.ac.cn, gcguo@fjirsm.ac.cn Fax: +86-591-83714946; Tel: +86-591-83705882

<sup>b</sup> College of Chemistry, Fuzhou University, Fuzhou, Fujian, 350116, P. R. China

## **S1. Materials**

Bismuth nitrate pentahydrate (AR), Cerium nitrate hexahydrate (AR) 1,4-Naphthalenedicarboxylic acid (Aladdin, AR, 99%), imidazole (TCI, AR, 98%), potassium bicarbonate (MACKLIN, 99.99%), Nafion (Alfa Aesar, 5wt%), dimethyl sulfoxide (GENERAL-REAGENT, AR, 99%), and deuterium oxide (CIVI-CHEM, 99.9%) were used as received without further purification. N,N-dimethylformamide (AR) and absolute ethyl alcohol (AR) were purchased from Sinopharm Chemical Reagent Co, Ltd. Carbon paper (TGP-H-060, Toray) was used to prepare working electrode. Cationic ion exchange membrane Nafion 117 was purchased from DuPont (Wilmington, DE, USA). CO<sub>2</sub> (99.999%), Ar (99.99%) and gas mixture of H<sub>2</sub> /Ar (90:10 vol%) were purchased from the Yuanhua gas company. All aqueous solutions were prepared with Milli Q ultrapure water (18.2 MΩ·cm)

## **S2. Experimental Details**

### **S2.1 Synthesis of Bi-MOFs and Cerium-doped Bi-MOFs**

The Bi based metal-organic framework used as precursor (denoted as Bi-P1) for Bi@BiO<sub>x</sub>/C was synthesized via a solvothermal method. Typically, 0.6 mmol Bi(NO<sub>3</sub>)<sub>3</sub>·5H<sub>2</sub>O, 4 mmol 1,4-Naphthalenedicarboxylic acid and 0.6 mmol imidazole were dispersed in 16 mL DMF under continuous magnetic stirring (600 rpm) at room temperature. The mixture was then heated up to 90 °C and maintained for 72 h. The final product was collected by centrifugation and washed several times with DMF and absolute ethyl alcohol. Finally, the Bi-P1 white powder was dried in vacuum at 60 °C for 8 h. The dry white sample was collected for further use. The synthetic procedure of Cerium-doped Bi based metal-organic framework precursor (denoted as Ce-Bi-P1) for Ce-Bi@CeBiO<sub>x</sub>/C was similar to that of Bi-P1 except that the 0.6 mmol Bi(NO<sub>3</sub>)<sub>3</sub>·5H<sub>2</sub>O was replaced by 0.54 mmol Bi(NO<sub>3</sub>)<sub>3</sub>·5H<sub>2</sub>O and 0.06 mmol Ce(NO<sub>3</sub>)<sub>3</sub>·6H<sub>2</sub>O.

### **S2.2 Synthesis of Bi@BiO<sub>x</sub>/C and Ce-Bi@CeBiO<sub>x</sub>/C**

The as synthesized Bi-P1 and Ce-Bi-P1 precursors were firstly annealed at 200°C for 2 h and then the temperature was increased and kept at 500 for another 2 h. The heating

rate was controlled at 3 °C/min and the whole process was carried out under a reduction atmosphere of H<sub>2</sub>/Ar (90:10 vol%, 30 mL/min). Then, as the as-prepared black samples were ground and collected for further use.

### **S2.3 Preparation of electrodes**

To prepare the working electrode, the substrate of carbon paper was dipped in absolute ethyl alcohol for 60 minutes to remove impurities before using. 20 mg of catalyst was dispersed in a mixed solution of 275 μL of deionized water, 275 μL absolute ethyl alcohol and 55 μL of Nafion solution (5% wt) by sonicating for 0.5 h to form a homogeneous ink. The mixture was then dropped onto a carbon paper of 1 cm<sup>2</sup> to make sure the catalyst loading was 4 mg cm<sup>-2</sup>.

### **S2.4 Physicochemical characterization**

Scanning electron microscopy (SEM) images were obtained from a JSM6700-F microscope integrated with energy dispersive spectroscope (EDS) operating at 15 kV. Transmission electron microscopy (TEM), high angle annular dark field scanning transmission electron microscopy (HAADF-STEM) characterizations were performed in a Talos-F200X field emission transmission electron microscope operating at an acceleration voltage of 200 kV. The phase structures were examined by X-ray diffraction (XRD), which were obtained with a MiniFlex600 diffractometer (Rigaku) fitted with Cu Kα ( $\lambda = 1.5406 \text{ \AA}$ ) radiation in reflection mode from 5° to 80°. X-ray photoelectron spectroscopy (XPS) was performed on an Escalab 250 spectrometer (VG Systems) equipped with an Al-Kα (1486.7 eV) anode as an X-ray source. The standard C1s value of 284.8 eV was used to correct all reported XPS spectra. Electron spin resonance (EPR) spectra were recorded on a Bruker ER-420 spectrometer with a 100 kHz magnetic field in the X band at room temperature. The content of Bi in different catalysts was determined by an inductively coupled plasma spectrometer (ICP, Ultima2).

### **S2.5 Electrochemical measurements and product analysis**

Except the electrochemical impedance spectroscopy (EIS) measure, all the electrochemical measurements of the catalysts were conducted with Bio-Logic VMP3 at room temperature. EIS measurements (performed at open circuit potential with a frequency from 1000000 Hz to 0.01 Hz) were completed in a conventional three-electrode glass cell in 0.5 M  $\text{KHCO}_3$  aqueous solution with CHI920D. All the other electrochemical experiments were performed in the H-type gas tight cell with two-compartments separated by a cation exchange membrane (Nafion 117, Dupont). The prepared Bi-based electrodes and platinum plate were served as working and counter electrodes, respectively.

The electrolyte was bubbled with  $\text{CO}_2$  before the electrochemical tests for at least 30 minutes and then the flow rate of  $\text{CO}_2$  was changed to 10 sccm during the whole test process (pH =7.4). Linear sweep voltammetry (LSV) was carried out at a scan rate of 50 mV/s. During chronoamperometric test, the gas products from the cell was introduced directly to the gas sample loop of gas chromatograph (GC), which equipped with 2 of Porapak-N, C13 and SE30 columns for quantifications. The gas-phase product was analyzed by GC every 5 minutes. CO in the gas products was analyzed by flame ionization detector (FID) after conversion by methane reformer while  $\text{H}_2$  in the gas products was analyzed by thermal conductivity detector (TCD). The liquid products were characterized by  $^1\text{H}$  nuclear magnetic resonance ( $^1\text{H}$ -NMR) spectra. Typically, 0.49 mL electrolyte after electrolysis was mixed with 0.1 mL  $\text{D}_2\text{O}$ , and 0.01 mL dimethyl sulfoxide (DMSO) water solution (1%, v%) was added as an internal standard. The one-dimensional  $^1\text{H}$  spectrum was measured with water suppression using a solvent pre-saturation technique.

The stability test was carried out at the potential of  $-1.6$  V vs. SCE for 10 h.  $\text{CO}_2$ -saturated 0.5 M  $\text{KHCO}_3$  aqueous solution was replaced by Ar-saturated 0.5 M  $\text{KHCO}_3$  aqueous solution for checking that the formate was produced from the reduction of  $\text{CO}_2$  rather than the decomposition of  $\text{HCO}_3^-$ .

Tafel slopes for formate production were calculated from the corresponding geometric current densities and the formate Faradaic efficiency.

The electrochemical surface area (ECSA) was obtained by the double-layer capacitance

method using the follow equation:

$$ECSA = C_{dl}/C_s$$

where  $C_{dl}$  is the double-layer capacitance measured by cyclic voltammetry (CV) method with different scan rates at the potential from -0.93 to 0.66 V.  $C_{dl}$  was determined from the plot slope of the double-layer charging current versus the scan rate.  $C_s$  is the specific capacitance which value is  $40 \mu\text{F cm}^{-2}$  used in this work.

## S2.7 Calculation of Faradaic Efficiency

### S2.7.1 Liquid products

$$FE_{liquid} = V \times c \times \frac{nF}{Q}$$

$V$ : the volume of the electrolyte in the working cell;

$c$ : the concentration of liquid product after electrolysis, determined by  $^1\text{H NMR}$ ;

$n$ : number of transferred electrons for certain product;

$F$ :  $96485 \text{ C mol}^{-1}$ ;

$Q$ : total charge consumed in the electrolysis.

### S2.7.1 Gaseous products

$$FE_{gas} = V_t \times v \times \frac{nFP^0}{RT^0 I_t}$$

$V_t$ : the volume concentration of  $\text{H}_2$  or  $\text{CO}$  based on a calibration of the GC;

$n$ : number of transferred electrons for certain product;

$F$ :  $96485 \text{ C mol}^{-1}$ ;

$p^0$ :  $101.3 \text{ kPa}$ ;

$R$ : Gas constant in  $\text{JK}^{-1}\text{mol}^{-1}$

$T^0$ : the temperature for testing;

$I_t$ : the steady-state current measured during a constant-potential electrolysis.

## S2.8 Randles–Sevcik equation

$$i_p = 0.4463nFAC\left(\frac{nFvD}{RT}\right)^{\frac{1}{2}}$$

If part of the parameters are controlled, the equation could be simplified as follow

$$i_p = kD^{\frac{1}{2}} \times v^{\frac{1}{2}}$$

$i_p$ : current maximum in amps

$n$ : number of electrons transferred in redox event

$A$ : electrode area in  $\text{cm}^2$

$F$ :  $96485 \text{ C mol}^{-1}$ ;

$D$ : diffusion coefficient in  $\text{cm}^2/\text{s}$

$C$ : concentration in  $\text{mol}/\text{cm}^3$

$v$ : scan rate in  $\text{V}/\text{s}$

$R$ : Gas constant in  $\text{JK}^{-1}\text{mol}^{-1}$

$T$ : temperature in K

### Supplementary figures

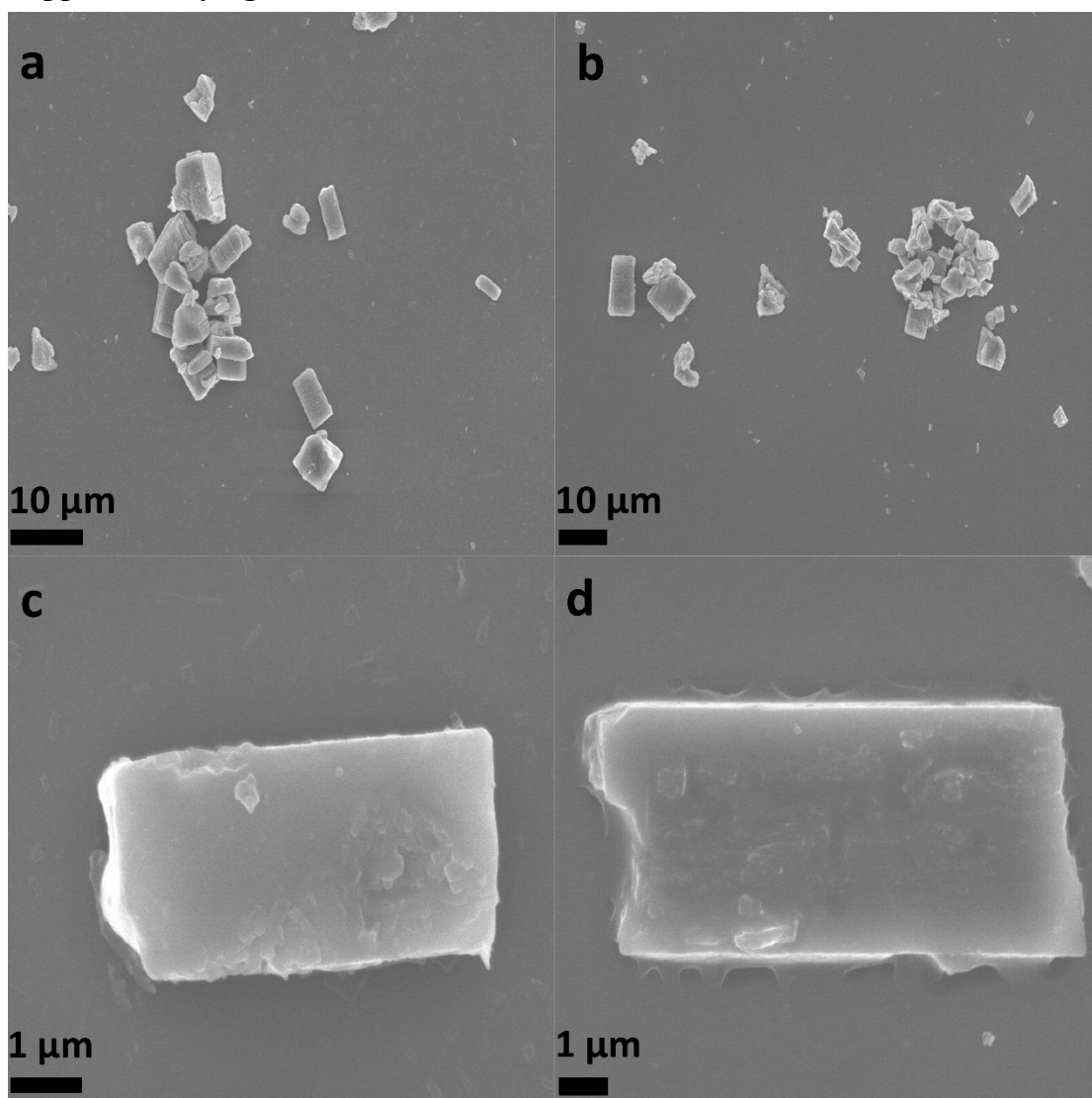


Fig. S1. SEM images with different magnifications of Bi-P1 precursor (a, c), and Ce-Bi-P1 precursor (b, d).

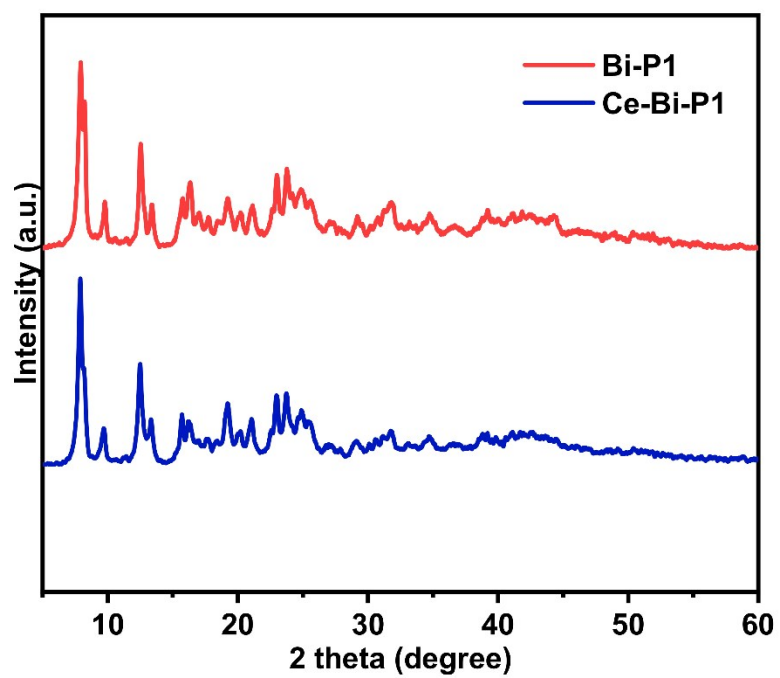


Fig. S2. XRD patterns of Bi-P1 and Ce-Bi-P1 precursors.

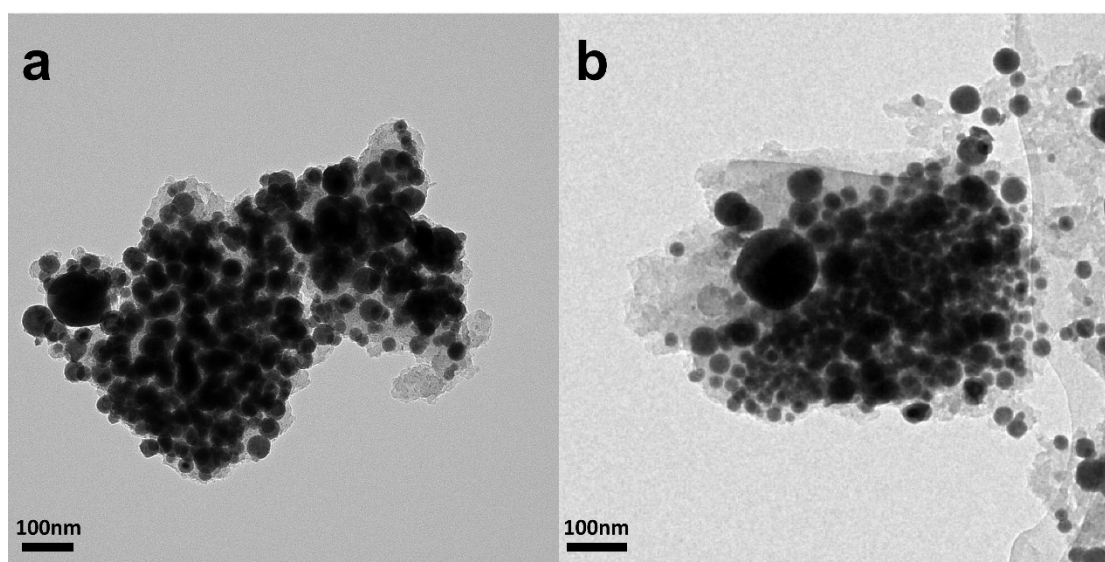


Fig. S3. TEM images of a) Ce-Bi@CeBiO<sub>x</sub>/C and b) Bi@BiO<sub>x</sub>/C

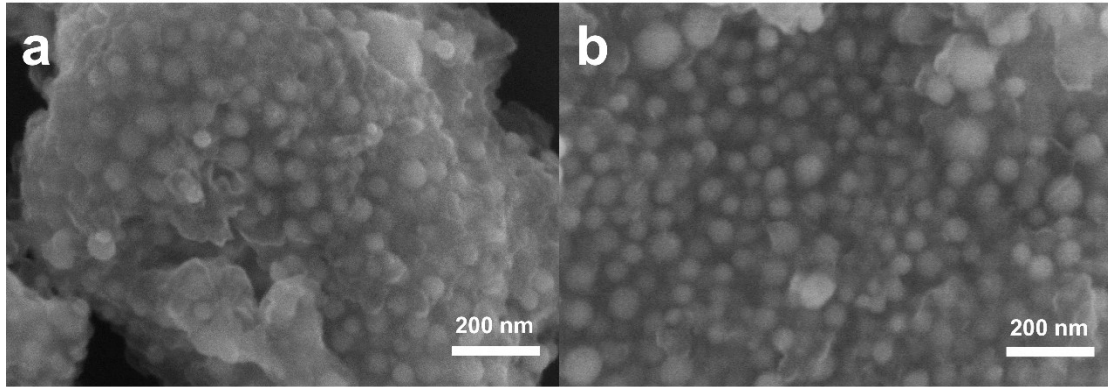


Fig. S4. SEM images of Bi@BiO<sub>x</sub>/C and Ce-Bi@CeBiO<sub>x</sub>/C

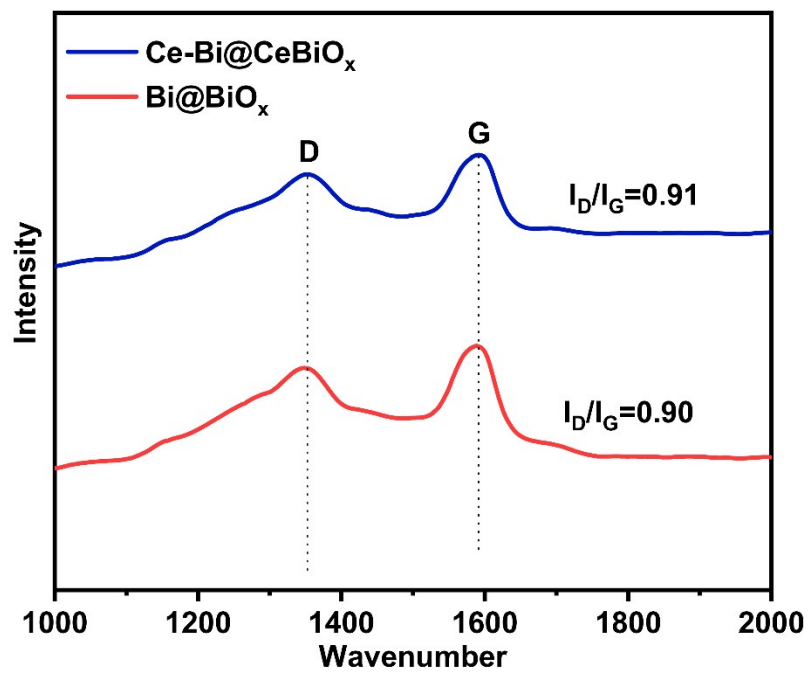


Fig. S5. Raman spectra of Bi@BiO<sub>x</sub>/C and Ce-Bi@CeBiO<sub>x</sub>/C

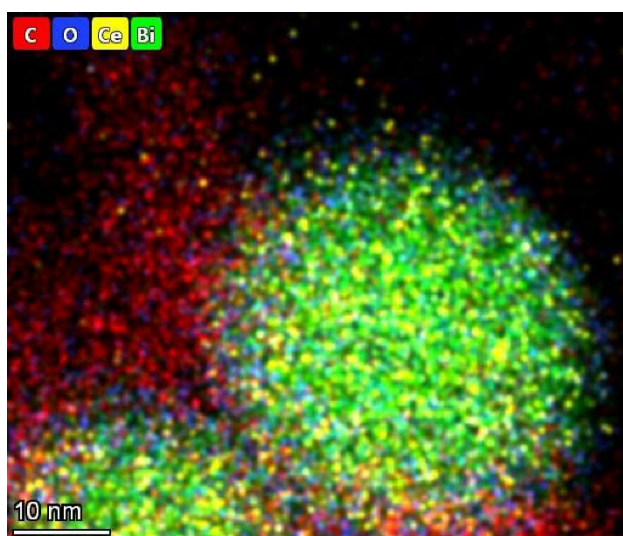


Fig. S6. Element mapping for all elements of Ce-Bi@CeBiO<sub>x</sub>/C

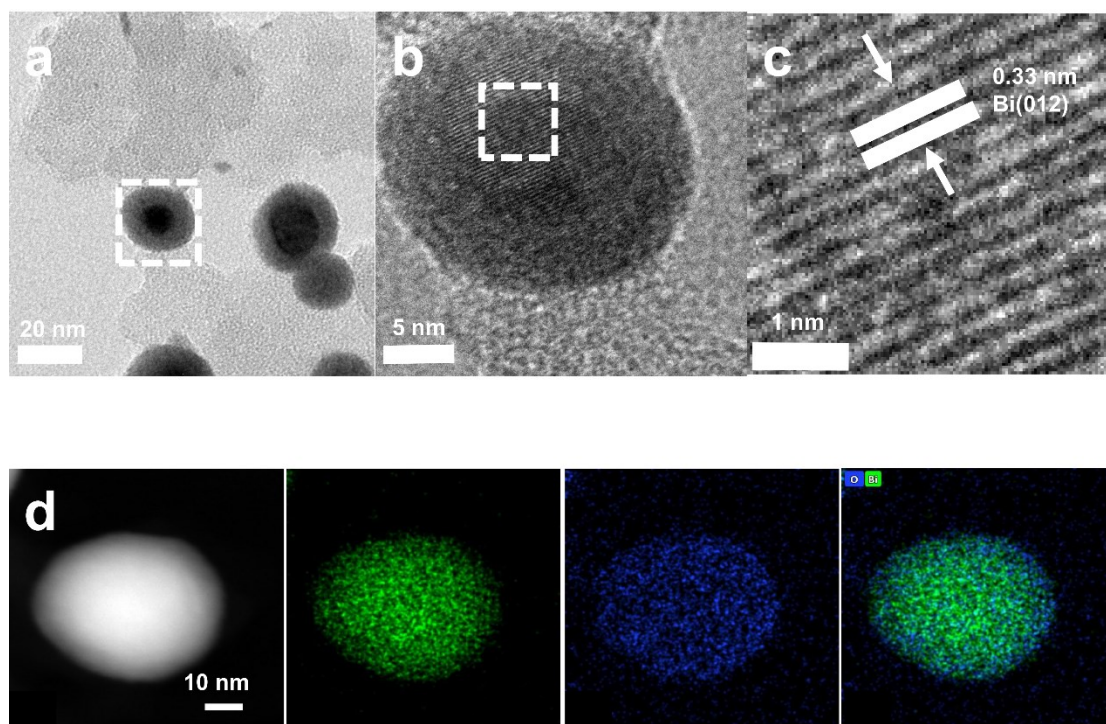


Fig. S7. a) HRTEM images of Bi@BiO<sub>x</sub>/C; b) and c) is a magnification of the white squares in a) and b) respectively; d) EDS elemental mappings of Bi@BiO<sub>x</sub>/C.

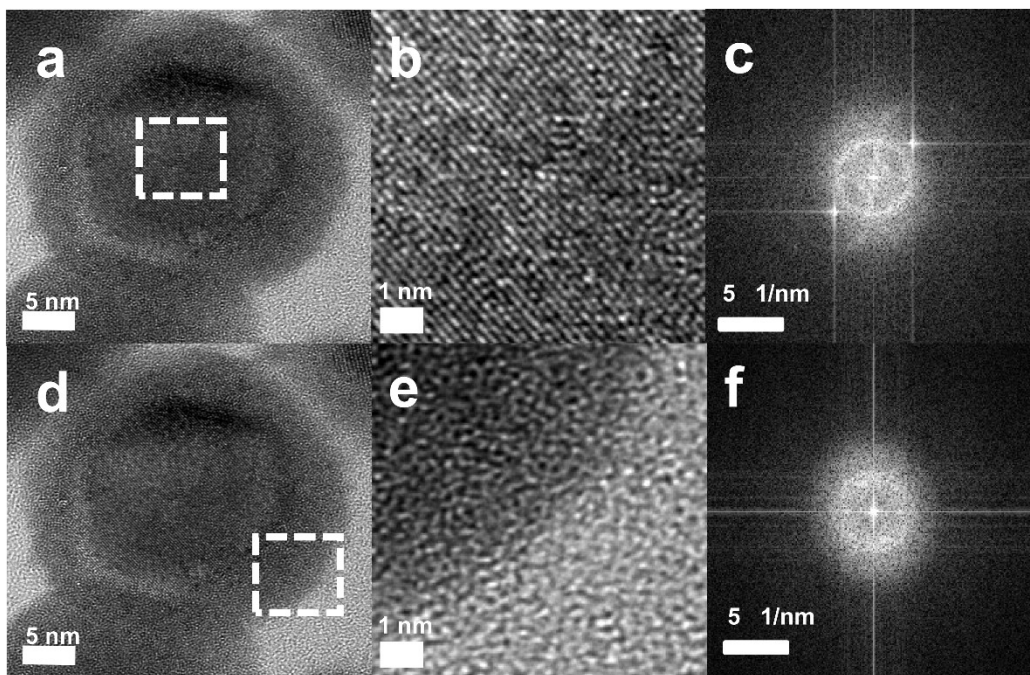


Fig. S8. a,d) HRTEM images of Ce-Bi@CeBiO<sub>x</sub>/C; b) and e) is a magnification of the white squares in a) and d) respectively; c,f) the corresponding FFT images of b) and e).

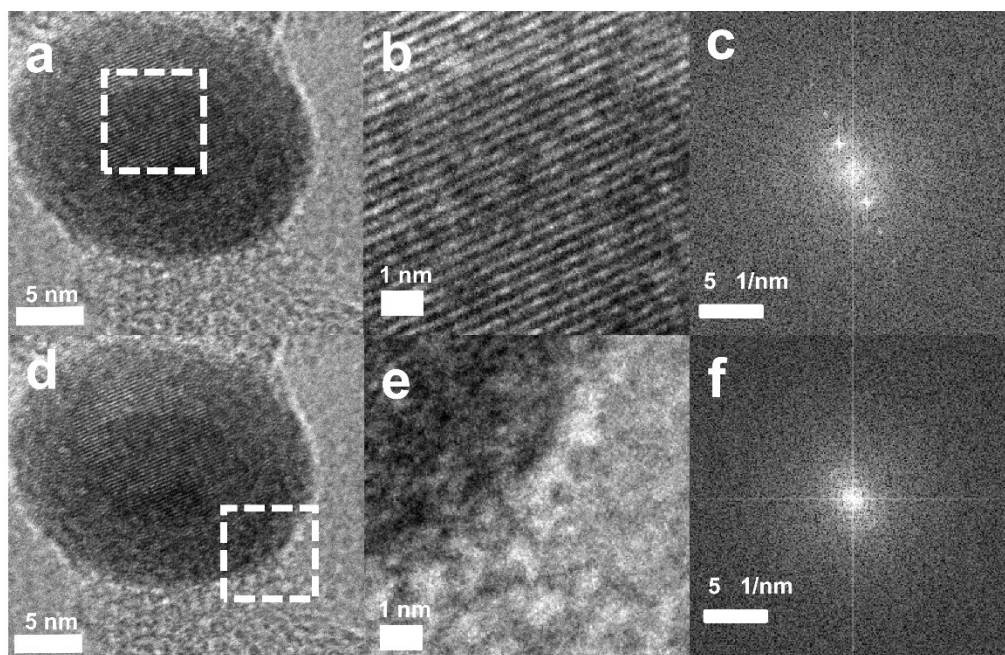


Fig. S9. a,d) HRTEM images of Bi@BiO<sub>x</sub>/C; b) and e) is a magnification of the white squares in a) and d) respectively; c,f) the corresponding FFT images of b) and e).

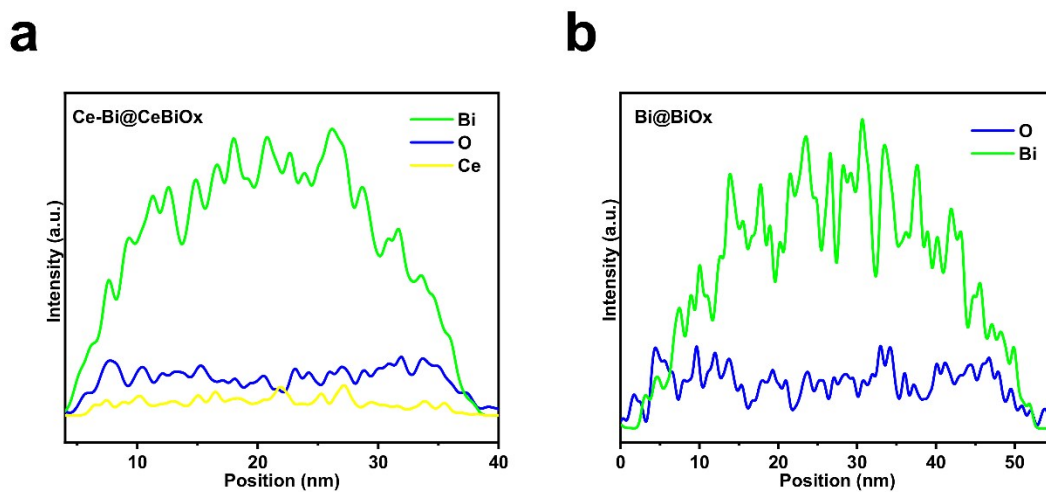


Fig. S10. EDS line scan Ce-Bi@CeBiO<sub>x</sub>/C and b) Bi@BiO<sub>x</sub>/C

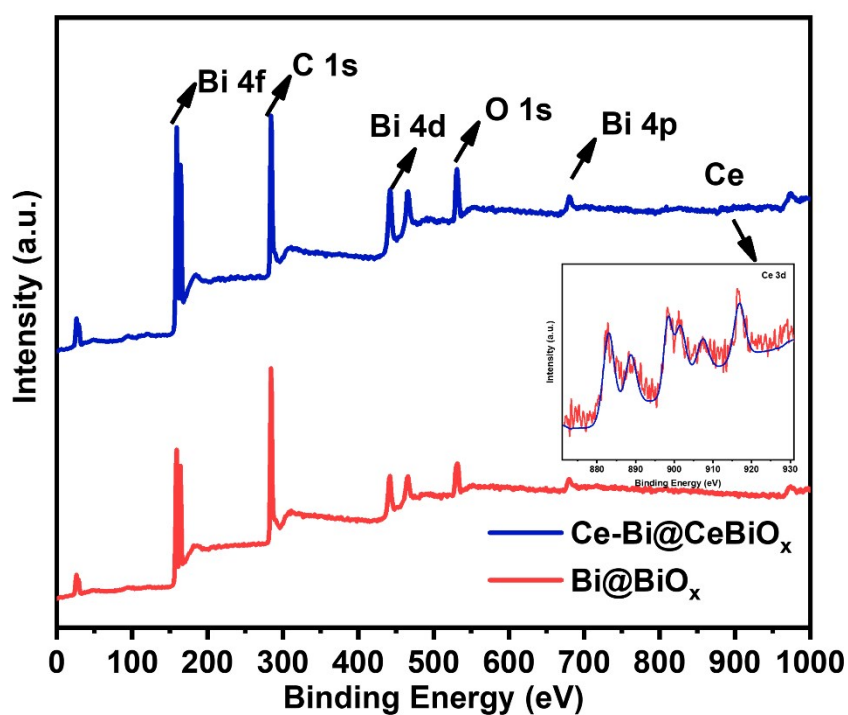


Fig. S11. XPS survey spectra of Bi@BiO<sub>x</sub>/C and Ce-Bi@CeBiO<sub>x</sub>/C (the inset shows the Ce 3d spectrum of Ce-Bi@CeBiO<sub>x</sub>/C)

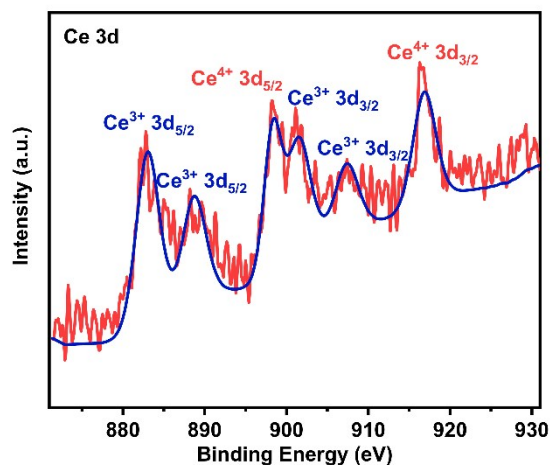


Fig. S12. Ce 3d spectrum of Ce-Bi@CeBiO<sub>x</sub>/C

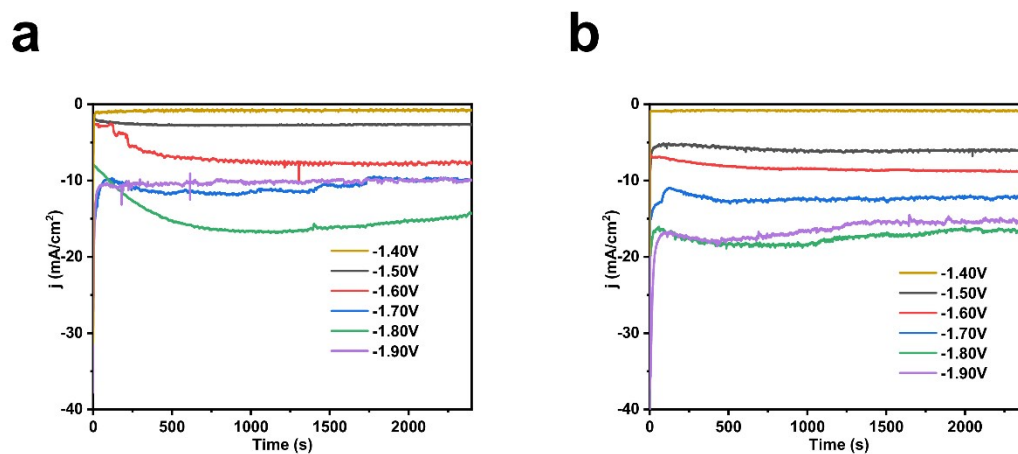


Fig. S13. Chronoamperometry curves of Bi@BiO<sub>x</sub>/C (a) and Ce-Bi@CeBiO<sub>x</sub>/C (b) at different applied potentials in CO<sub>2</sub>-saturated 0.5 M KHCO<sub>3</sub> solution.

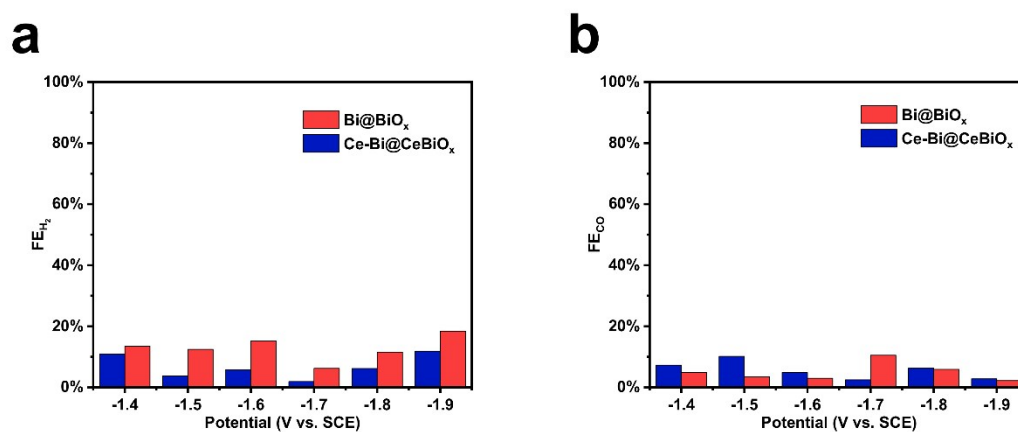


Fig. S14. FE of H<sub>2</sub> (a) and CO (b) for Bi@BiO<sub>x</sub>/C and Ce-Bi@CeBiO<sub>x</sub>/C.

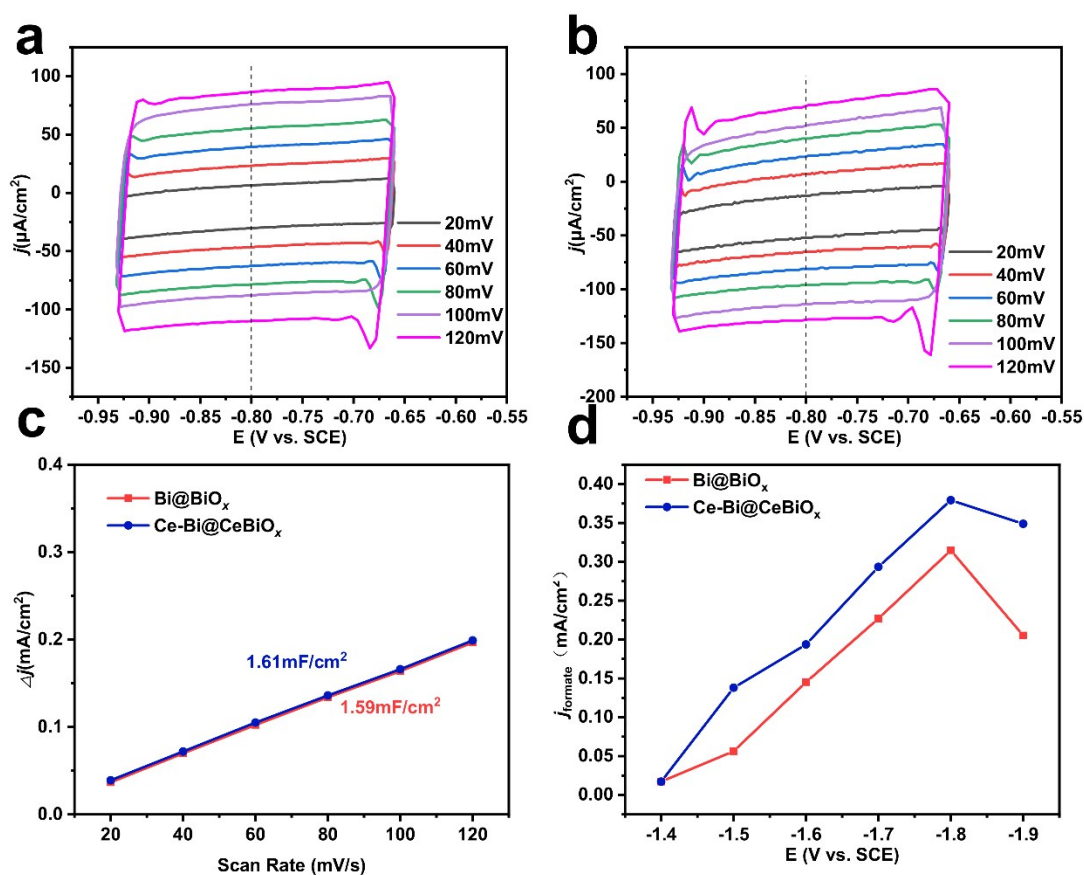


Fig. S15 CVs of a) Bi@BiO<sub>x</sub>/C and b) Ce-Bi@CeBiO<sub>x</sub>/C recorded at different scan rates in 0.5 M KHCO<sub>3</sub> electrolyte with a potential range from -0.93 V to -0.66 V.; c) The fitting plots of current densities versus scan rates for Bi@BiO<sub>x</sub>/C and Ce-Bi@CeBiO<sub>x</sub>/C, the current densities were obtained from the double layer charge/discharge curves at -0.80 V; d) Partial current densities of formate normalized by ECSA for Bi@BiO<sub>x</sub>/C and Ce-Bi@CeBiO<sub>x</sub>/C.

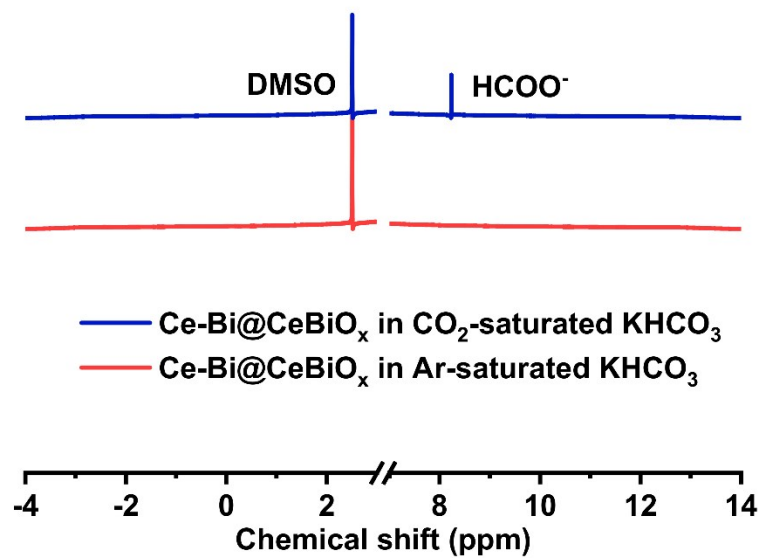


Fig. S16. <sup>1</sup>H NMR spectra of the electrolyte after electrolysis at -1.6 V vs. SCE for Ce-Bi@CeBiO<sub>x</sub>/C in CO<sub>2</sub>-saturated and Ar-saturated 0.5M KHCO<sub>3</sub> aqueous solution, respectively.

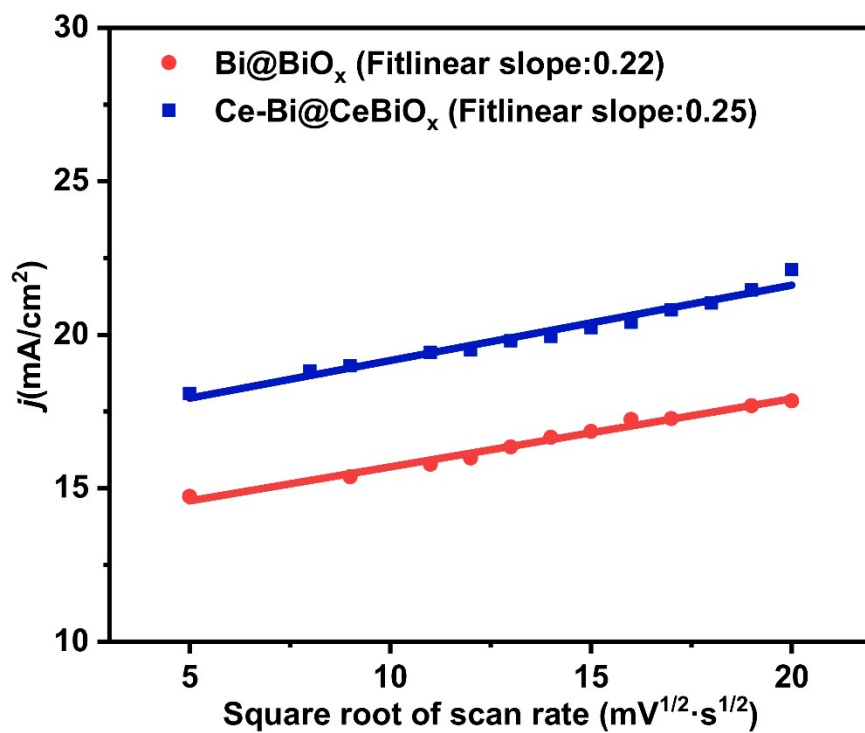


Fig. S17 Reduction current density at -1.8 V plotted against the square root of scan rate for Bi@BiO<sub>x</sub>/C and Ce-Bi@CeBiO<sub>x</sub>/C

Table S1. The ICP analysis of Bi, Ce in Bi@BiO<sub>x</sub>/C and Ce-Bi@CeBiO<sub>x</sub>/C

Elements	Ce (wt%)	Bi(wt%)
Bi@BiO <sub>x</sub> /C	-	61.48
Ce-Bi@CeBiO <sub>x</sub> /C	1.30	63.41

Table S2. Comparison of the performances for electrochemical reduction of CO<sub>2</sub> to formate on Ce-Bi@CeBiO<sub>x</sub> and those Bi-based catalysts reported in literatures.

Catalyst	<i>E</i> (vs. RHE)	FE <sub>formate</sub> (%)	<i>j</i> <sub>Formate</sub>	Ref
Ce-Bi@CeBiO <sub>x</sub>	-1.0V	96	11.8 mA cm <sup>-2</sup>	This work
	-1.1V	88	15.2 mA cm <sup>-2</sup>	This work
Bi <sub>2</sub> O <sub>3</sub> NSs@MCCM	-1.256 V	93.8	14 mA cm <sup>-2</sup>	1
BiOC nanosheets	-0.7 V	85	10.5 mA cm <sup>-2</sup>	2
defect-rich Bi	-0.75 V	84	5 mA cm <sup>-2</sup>	3
Bi/Cu	-1.07 V	95	6 mA cm <sup>-2</sup>	4
Bi nanosheets	-1.1 V	86	14.2 mA cm <sup>-2</sup>	5
Bi nanoparticle	-0.88V	90	6.5 mA cm <sup>-2</sup>	6
BiOCl <sub>0.5</sub> Br <sub>0.5</sub>	-0.93 V	98	9.47 mA cm <sup>-2</sup>	7
oxide-derived Bi films	-0.92 V	75	8.3 mA cm <sup>-2</sup>	8
BiOCl nanosheets	-0.83 V	92	3.4 mA cm <sup>-2</sup>	9
Bi <sub>45</sub> /GDE	-0.80 V	90	1.3 mA cm <sup>-2</sup>	10
Bi dendrite	-0.74 V	89	2.3 mA cm <sup>-2</sup>	11
5 nm SnO <sub>2</sub> nanoparticles	-1.189 V	93	10.8 mA cm <sup>-2</sup>	12
nanoporous Sn/SnO <sub>2</sub> composites	-1.1 V	80	12.8 mA cm <sup>-2</sup>	13

## Reference

- 1 S. Liu, X. F. Lu, J. Xiao, X. Wang and X. W. Lou, *Angew. Chemie - Int. Ed.*, 2019, **58**, 13828–13833.
- 2 Y. Zhang, X. Zhang, Y. Ling, F. Li, A. M. Bond and J. Zhang, *Angew. Chemie - Int. Ed.*, 2018, **57**, 13283–13287.
- 3 Y. Zhang, F. Li, X. Zhang, T. Williams, C. D. Easton, A. M. Bond and J. Zhang, *J. Mater. Chem. A*, 2018, **6**, 4714–4720.
- 4 W. Lv, J. Zhou, J. Bei, R. Zhang, L. Wang, Q. Xu and W. Wang, *Appl. Surf. Sci.*,

- 2017, **393**, 191–196.
- 5 W. Zhang, Y. Hu, L. Ma, G. Zhu, P. Zhao, X. Xue, R. Chen, S. Yang, J. Ma, J. Liu and Z. Jin, *Nano Energy*, 2018, **53**, 808–816.
  - 6 X. Zhang, X. Hou, Q. Zhang, Y. Cai, Y. Liu and J. Qiao, *J. Catal.*, 2018, **365**, 63–70.
  - 7 Y. Qiu, J. Du, W. Dong, C. Dai and C. Tao, *J. CO2 Util.*, , DOI:10.1016/j.jcou.2017.05.024.
  - 8 E. Bertin, S. Garbarino, C. Roy, S. Kazemi and D. Guay, *J. CO2 Util.*, 2017, **19**, 276–283.
  - 9 H. Zhang, Y. Ma, F. Quan, J. Huang, F. Jia and L. Zhang, *Electrochem. commun.*, 2014, **46**, 63–66.
  - 10 X. Zhang, T. Lei, Y. Liu and J. Qiao, *Appl. Catal. B Environ.*, 2017, **218**, 46–50.
  - 11 J. H. Koh, D. H. Won, T. Eom, N. K. Kim, K. D. Jung, H. Kim, Y. J. Hwang and B. K. Min, *ACS Catal.*, 2017, **7**, 5071–5077.
  - 12 S. Zhang, P. Kang and T. J. Meyer, *J. Am. Chem. Soc.*, 2014, **136**, 1734–1737.
  - 13 S. Liu, F. Pang, Q. Zhang, R. Guo, Z. Wang, Y. Wang, W. Zhang and J. Ou, *Appl. Mater. Today*, 2018, **13**, 135–143.